A SURFACE-WAVE INVESTIGATION OF THE RUPTURE MECHANISM OF THE GOBI-ALTAI (4 DECEMBER 1957) EARTHQUAKE.

Emile A. Okal

Seismological Laboratory, California Institute of Technology,
Pasadena, California 91125

Abstract :

Long-period records of multiple Love waves from the 1957 earthquake in Mongolia (M_S = 8.0) at Pasadena are analyzed and compared to synthetic seismograms, generated by the method of Kanamori (1970a,b). A fit in the time domain shows that the records are not consistent with the previous solution, achieved through a frequency-domain analysis of directivity by Ben-Menahem and Toksöz (1962). The solution asks for a shorter rupture of 270 km at a velocity of 3.5 km/s. The focal parameters are constrained by updating all the reported first-motion and are found to be : Strike = 103°, Dip = 53°, Slip = 32°. A seismic moment of $1.8\ 10^{28}$ dynes-cm is obtained. These figures are also consistent with a time-domain analysis of Love waves at Palisades and Strasbourg, and of Rayleigh waves at Pasadena, with a directivity study of Love waves at Pasadena, and with static deformation and isoseismal data. A discussion is given of the relation between moment, magnitude and rupture area, and a comparison is made with other events in the same region: It is concluded that this earthquake does not exhibit an "intra-plate" behavior, but rather compares better with "inter-plate" events, such as the great Assam earthquake.

Introduction :

At 03:37:45.0 TU, on December 4, 1957, a major earthquake (M_s = 8.0) occurred along the Bogdo fault in central Mongolia. The epicenter was subsequently computed at 45.3 ± 0.2 °N by 99.3 ± 0.15 °E (Florensov and Solonenko, 1963). Although this event, known as the Gobi-Altai earthquake, did little civilian damage, due to its location under desert mountain ranges (Fig. 1), it was soon recognized as one of the major earthquakes in recent times, and an extensive field investigation was conducted by a team of Russian and Mongolian scientists (Florensov and Solonenko, 1963).

Furthermore, in view of the recent advent of plate tectonics, this earthquake could be regarded as the largest recent expression of intra-plate seismicity. It is therefore challenging to thoroughly investigate its mechanism. The only such attempt had been made by Ben-Menahem and Toksoz (1962) [hereafter referred to as BMT62], who studied multiple Rayleigh waves R_3 to R_6 recorded at Pasadena. However, at the time, the theory of surface-wave excitation was not fully developed and their study was focused on an investigation of directivity in the frequency domain. Their results asked for a fault rupture of 560 km, striking N100°E, at a rupture velocity of 3.5 km/s. The development of long-period surface-wave synthetic seismograms (Kanamori, 1970a,b) allows a time-domain investigation of the rupture mechanism and warrants a complete reassessment of the focal and rupture process of the Gobi-Altai event.

In Section 1, we discuss the focal solution of the earthquake, before determining the rupture process in section 2. A discussion of directivity effects is given in section 3. A computation of the seismic

moment is given in section 4, and this figure is discussed with respect to general intra-plate tectonics.

1. Focal process.

The focal process of the Gobi-Altai earthquake has long been a challenge. At the time of the BMT62 paper, the solution could only be inferred from surface deformation data. Hodgson et al.(1962) noted a high degree of inconsistency among the first-motion reports. They proposed a mechanism shown on Figure 2a, with strike (ϕ), dip (δ) and slip (λ) angles of respectively 125.5, 55, and 24.3 degrees. Florensov and Solonenko (1963) show that their solution [$\phi = 107°$, $\delta = 41°$, $\lambda = 40°$] is rather poorly constrained, the azimuths of the planes, for example, being allowed to vary 35° around the chosen values (Figure 2b). They also report inconsistencies in first-motion data. In view of the location of the station PAS (its azimuth from the direction of the fault varies from 60° to 95° depending on the model), it is crucial to achieve a better solution, if one is build synthetic seismograms. This is made possible by including mostly dilatational data from Indian stations (BOM, HYB, CCU, KOD), which were not used by Florensov and Solonenko, and mostly compressional data from Central Asia (DSB, KIR, AND, LAH), which were not used by Hodgson et al.

Inclusion of these data points yields a better-constrained solution: $\phi = 103°$, $\delta = 53°$ and $\lambda = 32°$, shown on Figure 2c. The rather large number of inconsistencies, mostly from European stations, may be due to the fact that most European stations lie in the direction opposite to faulting, and therefore give rise to emergent records. The long-period Galitsin record at DBN clearly shows a compression on Z, and a SW first motion on the horizontal instruments. Similar records at FIR also agree, as do both short- and long-period records at STR. Records

at UCC show a self-inconsistent (Down, South, West) first motion. However, the shape of the signal is very similar to that at DBN (the two stations are only 150 km apart) and it is believed that the polarity of the Z instrument at UCC was wrong. This set of data clearly puts Western Europe into a compressional quadrant. The data from India and Central Asia constrains the solution to within a few degrees. It should be noted that the proposed solution, which represents a left-lateral strike-slip with a fair amount of thrust (see figure 2d), is consistent with the surface-rupture studies quoted from Florensov (1958) in BMT62. The solution is also basically consistent with the general pattern of Asian Tectonics, as described by Molnar and Tapponnier (1975).

2. Rupture process from time-domain surface wave studies.

Records used in this study were principally those obtained at PAS, by the high-pass "30-90" 3-component seismometer (Press et al., 1958), and by the low-gain strainmeter. Additional Press-Ewing records from PAL and Galitsin records from STR were also used. Table 1 lists some parameters of the stations and records used in this study. The particular azimuthal location of PAS with respect to the fault elements is favorable to Love rather than Rayleigh waves.

Love waves at Pasadena: Records of the three components of the 30-90 instrument were digitised from 06:44 to 14:00 TU, and the horizontal ones were rotated into SH polarization. The phases G_3, G_4, and G_5 were isolated and equalised to a station distance of 90 degrees. Components with periods lower than 60 sec. were at the same time removed. No attempt to process G_6 and G_7 was made, although these phases were readily identifiable on the records (see figure 3). The computation of the synthetic

seismograms followed the procedure described by Kanamori and Cipar (1975). Several lengths of rupture were used, varying from 200 km to 560 km, this upper limit being the rupture length proposed by BMT62. A rupture velocity of 3.5 km/s, similar to that used in BMT62, was used throughout the study. A step-function type of source was chosen, and no attenuation of the source along the rupture was assumed. In section 3, we will discuss part of this last hypothesis on the basis of some directivity data. The azimuth of propagation of the faulting was taken to coincide with the trace of the fault plane ($\phi = 103°$).

Synthetics for G_3, G_4 and G_5 are shown on Figure 4, for fault lengths of 560 km (suggested by BMT62) and 270km (which turned out to give the best fit to our data), and are compared with the observed traces. It is readily seen that a fault length of 560 km cannot account for the observed wave shapes: The frequency content of the synthetic G_3 and G_5 is clearly different from that of the observed phases, and the shape of the synthetic G_4 exhibits a doublet, due to a rupture propagation backwards from the departing wave. On the other hand, a length of 270 km gives a most satisfactory fit to G_3, and also to G_5 and G_4, although the amplitude of G_4 remains somewhat too large.

Rayleigh waves at Pasadena.

Synthetics were computed for the phase R_3 at PAS. It was found that the length of the rupture has a rather limited influence on its waveshape and that R_3 cannot help in discriminating between various rupture lengths. The horizontal component of the phase R_2, recorded on the low-gain strain instrument, was also used: This system is equivalent to a mechanical seismometer with $T_s = 90$ sec. Figure 5 compares the observed

wave, filtered at T = 50 sec., with synthetics for both 270 and 560 km. As can easily be seen, the shape of R_2 at PAS is inconsistent with the 560 km fault length. This is important, because Rayleigh waves were the only data used in BMT62.

Other records.

Figure 6 shows a similar comparison between observed and synthetic seismograms for G_3 at PAL. The other records obtained were those at DBN, FIR, UCC, and STR; these stations are located at an azimuth extremely unfavorable to Rayleigh waves, and, indeed, those are not easily observed on the records. The best record was that of G_2 at Strasbourg (Figure 7). Unfortunately, it does not help /discriminate between rupture lengths, because of station azimuth. This point will be discussed in the next section.

As a partial conclusion to this section, it can be stated that most of the records of both G and R waves are incompatible with a rupture length of 560 km, whereas all agree with a shorter length of 270 km at 3.5 km/s.

3. Frequency-domain investigation.

Our results conflict with those from BMT62, which were obtained in the frequency domain. In order to examine the cause of this discrepancy, we analysed our data in the frequency domain, and made a directivity plot similar to that of BMT62, for G_3/G_4 at PAS. The theoretical aspects of the problem of the directivity function of a moving source have been described by Ben-Menahem (1961), who showed that a spectral component of frequency f, leaving the source at an angle θ from the rupture direction, is attenuated by an amount :

$$(1) \qquad D(\theta) = \left| \frac{\sin \frac{\pi \ell f}{c} (c/v - \cos\theta)}{\frac{\pi \ell f}{c} (c/v - \cos\theta)} \right| ,$$

where ℓ is the rupture length, v the rupture velocity and c the surface-wave phase velocity at frequency f. For two successive multiple surface waves, such as G_3 and G_4, at the same station, equalised to an identical distance, the spectral ratio is then given by:

$$(2) \qquad \frac{D(\theta)}{D(\theta + \pi)} = \left| \frac{c/v + \cos\theta}{c/v - \cos\theta} \cdot \frac{\sin \frac{\pi \ell f}{c} (c/v - \cos\theta)}{\sin \frac{\pi \ell f}{c} (c/v + \cos\theta)} \right|$$

The experimental value of this ratio for G_3/G_4 at PAS is shown on Figure 8 and is compared with theoretical models for both fault lengths. Should the fault be 560 km long, a peak in the directivity function would be expected around 200 sec., for which there is no evidence in the data. On the other hand, a reasonably good agreement is found with the theoretical spectrum ratio for 270 km. This indeed is a conclusion similar to that in BMT62, in which the authors noticed the disapearrance of the expected first Rayleigh wave directivity peak. Although the gain of the instrument is rather low at these frequencies, both the present investigation and Figures 6 & 7 in BMT62 show that the amplitude of the spectrum of R_3, R_4, G_3 and G_4 is indeed maximum around 200 sec. It is therefore not possible to account for the non-existence of the 200 sec. peaks through errors introduced by the instruments.

Similarly, Figure 9 shows the spectrum of the R_2 record at PAS, on the long-period strain instrument. There is no evidence for the hole at T = 195 sec. required by the 560 km solution. The hole for 270 km falls in a rather rugged portion of the spectrum, for which no definite comment can be made. In the case of stations lying close to the azimuth opposite to the fault, such as most of the European stations (see Table 1), formula (1) shows easily that even-order waves, leaving the source in the direction of rupture will be affected by directivity only in the higher frequency part of their spectrum. The only odd-order wave record of good quality from Europe was that of G_1 at STR. However, its Fourier spectrum is rather rugged and does not indicate any definite directivity effect.

It is thus apparent that in the frequency domain, the analysis of directivity effects on Love and Rayleigh waves is not always a very powerful method of investigation of rupture mechanism. Difficulties in using this method were originally pointed out by Aki (1966). However, even in the Fourier space, most of the results from this study do agree better the shorter (270 km) length of the fault rather than with the longer (560 km) length suggested by BMT62. We were not able to find any evidence for the fundamental hole expected around 200 sec. in G_{2n} or R_{2n}, in a 560 km-length model. We would also like to point out that BMT62 used a data set of 2160 sec, which they extended to 20,000 sec. by adding zeroes. Therefore, their interval of sampling in the frequency domain cannot be shorter than $4.6\ 10^{-4}$ Hz = 1/(2160 sec.), and any feature of their spectra not extending over such an interval has no real physical meaning. It shoud be noted that many of the spikes in Figure 11 of BMT62 do not meet this criterion. Our analysis used a FFT over data samples of 2048 sec., and no substantial number of zeroes were added.

It therefore appears that the first peak of the directivity function, which Ben-Menahem and Toksoz identified as the #2-harmonic for a 560 km rupture, is in fact the fundamental for a 270 km fault.

As a conclusion to this section, it should be noted that the directivity plot on Figure 8 clearly shows strong spikes, extending over 3 orders of magnitude. This restricts the rupture process and helps reject both a bilateral fault and an attenuating source function, as was discussed in BMT62. Also, the aftershock pattern does not suggest a bilateral faulting. However, there does remain a trade-off between velocity of rupture and length of fault, which can be resolved neither in frequency nor in time domain. The discussion of some static data will put some further constrains on the possible solution.

4. Seismic moment and discussion:

The comparison of amplitudes between synthetic and observed seismograms allows a computation of the seismic moment of the earthquake. G_3 records at PAS yield a value of 1.8 10^{28} dynes-cm; R_3 at PAS yields 1.4 10^{28} dynes-cm; records at PAL ask for 2.3 10^{28} dynes-cm, although an accurate value of the gain of the instrument at this time was not available; the G_2 record at STR yields 1.4 10^{28} dynes-cm. A reasonable value is therefore $(1.8 \pm 0.4)10^{28}$ dynes-cm. It is interesting to compare this figure with the static data reported in Florensov and Solonenko (1963). These authors report average static dislocations along the fault on the order of 8 m. The depth of the hypocenter is estimated by them at 16 km. Continuous surface breakage asks for a vertical extent of at least 16 km, but probably not greater than 40 km. The width of the fault is then 20 to 50 km, due to the inclination of the fault plane, and the static moment $M = \mu SD$ is found to be 1.3 to 3.2 times 10^{28} dynes-cm, for a fault

length of 270 km, in agreement with the long-period seismic data.

Figure 10 is adapted from Florensov and Solonenko (1963) [their figure 89, p. 251 of the English translation]. It shows the distribution of the major aftershocks of the earthquake, and the line of isoseismic degree 5. Superimposed on it, we have plotted the 270 km and the 560 km faults. As can easily be seen, the 560 km fault would go well out of the isoseismic line. Although the data about this line was obtained in desert land and no continuation of it is available into China, its significance is not to be underestimated, in view of the extensive field work reported by Florensov and Solonenko (1963). On the same figure, it is easy to see that the repartition of aftershocks is confined to a length of about 300 km along the fault. Again, this is an indication supporting the 270 km hypothesis.

The magnitude of the Gobi-Altai earthquake has been computed by a number of agencies. The Bulletin of the Bureau International de Sismologie (Strasbourg) (1958 summarizes the surface-wave magnitudes reported by various observatories. A mean-value of $M_s = 8.04 \pm 0.45$ results. A redetermination from 20-sec. surface waves at PAS yields 7.98. A value of 8.0 has therefore been adopted here. It then becomes possible to compare the parameters of this earthquake with those of others, in the way of the study by Kanamori and Anderson (1975). The preceding sections suggest the following values: Magnitude $M_s = 8.0$; moment $M_o = 1.8\ 10^{28}$ dynes-cm; rupture surface $S = 10{,}000$ km^2

From these figures, it is possible to compute a stress drop $\Delta\sigma = 26$ bars, and an apparent stress $\eta\bar{\sigma} = 10.5$ bars. Although this last figure is not very accurate (and could probably vary from 3 to 30 bars), due to uncertainties in the magnitude-energy relation, it is still way under the average "intra-plate" apparent stress of 60 bars, determined

by Kanamori and Anderson (1975). In this respect, the Gobi-Altai earthquake plots among the inter-plate rather than intra-plate family on Figure 4 of Kanamori and Anderson's paper. Its next neighbors on the plot are the 1968 Tokachi-Oki, 1969 Kurile, 1970 Peru, 1944 Tonankai and 1946 Nankaido events, all major interplate earthquakes. The closest intraplate events are the 1952 Kern County and 1969 Portuguese earthquakes, which have much higher apparent stresses.

A similar result may be obtained from the stress drop $\Delta\sigma$. It should be emphasized that the relation between M_o and S, used in the determination of the stress drop, holds even for very large earthquakes, as pointed out by Kanamori and Anderson. On Figure 2 of their paper, the Gobi-Altai earthquake is comparable to the 1952 and 1968 Tokachi-Oki, 1966 Peru, 1969 Kurile, and 1944 Tonankai events. Again, intraplate events of comparable importance exhibit larger stress drops, and there seems to exist a major difference in terms of source parameters between the Gobi-Altai earthquake and other intra-plate events. In order to investigate this point furhter, we studied two other large events, which occurred in Mongolia and Sin-Kiang (Okal, 1976, to be published): The Urumtchi earthquake of 13 November 65, and the Khangai earthquake of 5 January 67 (see figure 1). The parameters of these events are listed on Table 2. Purposedly, they were chosen so that the seismotectonics involved in them are different from that of the Gobi-Altai earthquake: The Urumtchi earthquake is a thrust event between the Tien-Shan fold belt and the Dzungarian block; the Khangai event is a pure strike-slip presumably along a North-South fault (Molnar and Tapponnier, 1975), and possibly linked with the Lake Baikal rift system (Florensov, 1968). We also include in Table 2 the

results of Ben-Menahem et al.'s(1974) study of the great Assam earthquake of 15 August 50. Unfortunately, no data on fault dimensions is available for the Khangai and Urumtchi events, and only an apparent stress study can be made. Nevertheless, as can be seen, only the Khangai event clearly qualifies for intra-plate behavior. The Urumtchi earthquake has intermediate properties, and the Gobi-Altai event joins the Assam earthquake into the inter-plate family.

The interpretation of this feature is probably that the Bogdo fault, on which the Gobi-Altai event took place, is a major expression of present Eurasian tectonism, along which a major left-lateral slip of China towards the Pacific Ocean is taking place, as a result of the Himalayan collision, as proposed by Molnar et al. (1973) and Molnar and Tapponnier (1975), and possibly giving birth to a new "Chinese" plate.

This indeed raises the question whether there can exist any major ($M_S \geq 8.0$) intra-plate event, or whether such an event is large enough as to make the two sides of its fault separate entities on a world-wide scale. A very challenging project in this respect would be the investigation of the huge 1905 Mongolian events (M_S = 8.3 and 8.7 (?)) along the Bolnai fault. This might be done in the future, although the quality of the records involved is poor and a lot of uncertainty reigns over the characteristics of some of the instruments used at that time.

Conclusion:

We have shown that a time-domain analysis of surface waves from the Gobi-Altai earthquake suggests a fault length of 270 km, which is much shorter than previously determined. Results in the frequency domain suggest the same. The focal parameters (M_o = 1.8 10^{28} dynes-cm; M_s = 8.0) obtained from this study indicate that this earthquake has the characteristics of an inter-plate event, this being compatible with the present understanding of Chinese tectonics.

Acknowledgments.

I thank Professor Hiroo Kanamori for the use of his synthetic surface-wave programs, and for many discussions. I am grateful to Professor C.R. Allen, Editor of the English translation of Florensov and Solonenko (1963), who gave me permission to adapt figures 197 and 89 into figures 2b and 10 of the present paper. Seismic stations listed in Table 1 kindly provided originals or copies of the records used. This work was supported by NASA Contract NGL 05-002-069, and National Science Foundation Grant No. EAR 74-22489.

Contribution #2720 , Division of Geological and Planetary Sciences, California Institute of Technology.

References:

Aki, K., 1966 : Generation and propagation of G waves from the Niigata Earthquake of June 16, 1964; Part 1: A statistical analysis. Bull. Earth. Res. Inst., 44 , 23-72.

Ben-Menahem, A., 1961 : Radiation of seismic waves from finite moving sources. Bull. Seism. Soc. Am., 51 , 401-435.

Ben-Menahem, A., E. Aboodi and R. Schild, 1974 : The source of the great Assam earthquake : An interplate wedge motion. Phys. Earth Plan. Int., 9 , 265-289.

Ben-Menahem, A. and M.N. Toksöz, 1962 : Source mechanism from spectra of long-period seismic surface waves. Jnl. Geophys. Res., 67 , 1943-1955.

Bureau Central International de Sismologie, 1958 : Bulletin, Mois de Décembre 1957, p. 839, Strasbourg, 1958.

Florensov, N.A., 1958 : Catastrophic earthquake in the Gobi-Altai. Priroda, 7 , 73-77 (In Russian).

Florensov, N.A., 1968, Editor : The Baikal Rift Zone. Nauka, Moscow (In Russian).

Florensov, N.A. and V.P. Solonenko, 1963 : The Gobi-Altai Earthquake. Academy of Sciences of the USSR, Moscow. English Translation Israel Program for Scientific Translations, Jerusalem, 1965.

Hodgson, J.H., A.E. Stevens and M.E. Metzger, 1962 : Direction of Faulting in some of the larger earthquakes of 1956-57. Pub. Dom. Observ. Ottawa, 26 (4), 266-269.

Kanamori, H., 1970a : Synthesis of long-period surface waves and its applications to earthquake source studies — Kurile Islands earthquake of 13 October 1963. Jnl. Geophys. Res., 75 , 5011-5027.

Kanamori, H., 1970b : The Alaska earthquake of 1964: Radiation of Long-period surface waves and source mechanism. Jnl. Geophys. Res., 75 , 5029-5040.

Kanamori, H. and D.L. Anderson, 1975 : Theoretical Basis of some empirical relations in Seismology. Bull. Seism. Soc. Am., 65 , 1073-1096.

Kanamori, H. and J. Cipar, 1975 : Focal process of the great Chilean earthquake of May 22, 1960. Phys. Earth Plan. Int., 9 , 128-136.

Molnar, P., T.J. Fitch and F.T. Wu, 1973 : Fault plane solutions of shallow earthquakes and contempoarry tectonics in Asia. Earth Plan. Sci. Lett., 19 , 101-112.

Molnar, P. and P. Tapponnier, 1975 : Cenozoic Tectonics of Asia: Effects of a continental collision, Science, 189 , 419-426.

Press, F., M. Ewing and F.E. Lehner, 1958 : A Long-period seismograph system. EOS,Trans. AGU, 39 , 106-108.

TABLE 1.

List of stations and records used in the study of the Gobi-Altai Earthquake.

Code	Name and Country	Distance from epicenter (degrees)	Azimuth from epicenter (degrees)	Instruments.
PAS	Pasadena, Calif.	93.71	30.23	Press-Ewing (N,E,Z) Low-gain strainmeter (N,E)
PAL	Palisades, N.Y.	93.96	354.83	Press-Ewing (N,E,Z)
DBN	De Bilt, Netherlands	58.21	313.7	Galitsin (N,E,Z)
FIR	Firenze, Italy	59.57	303.04	Galitsin (N,E)
UCC	Uccle, Belgium	59.37	312.83	Galitsin (N,E,Z)
STR	Strasbourg, France	58.32	309.24	Galitsin (N,E,Z) Short-Period.

TABLE 2

Source parameters of Asian Earthquakes used in the present study.

Name	Date	Type	Epicenter (N,E)	M_s	M_o (dynes-cm)	Apparent stress (bars)	Stress drop (bars)
Gobi-Altai	4 Dec 57	Strike-Slip and thrust.	45.21 99.24	8.0	$1.8\ 10^{28}$	10.5	26
Khangai	5 Jan 67	Strike-slip	48.24 102.90	7.35	$3.2\ 10^{26}$	63	--
Urumtchi	13 Nov 65	Thrust	43.85 87.74	6.7	$8.3\ 10^{25}$	26	--
Assam (*)	15 Aug 50	Thrust	28.30 96.70	8.6	$2.5\ 10^{29}$	6	10

(*) Data from Ben-Menahem et al. (1974)

Figure Captions.

Figure 1. Map of Mongolia, showing locations and focal mechanisms of the Gobi-Altai (4 Dec 57) earthquake and of the two events mentioned in Section 4.

Figure 2. (a) Focal sphere plot of first-motion data obtained for the Gobi-Altai event by Hodgson et al. Black circles are compressions, open ones dilatations.
(b) Focal mechanism achieved by Florensov and Solonenko. Heavy lines indicate probable solution; dashed lines show possible uncertainty range. Black and open circles as in (a).
(c) Focal mechanism obtained in this study. Black and open circles as in (a).
(d) Scheme of focal dislocation. The arrow shows direction of movement of the hanging wall relative to the foot wall.

Figure 3. Transverse (SH-polarized) trace of the Press-Ewing record at PAS.

Figure 4. Observed and synthetic records of Love waves at PAS.
(a) Synthetic seismograms for a 560 km rupture length
(b) Synthetic seismograms for a 270 km rupture length
(c) Observed signals. The 560km G_4 synthetic has been shifted upwards to enhance clarity.

Figure 5. Observed and synthetic seismograms for the horizontal component of R_2 at PAS. (a),(b) and (c) as in figure 4.

Figure 6. Observed and synthetic seismograms for G_3 at PAL. (a),(b),and (c) as in figure 4.

Figure 7. Observed and synthetic seismograms for G_2 at STR. (a),(b) and (c) as in figure 4.

Figure 8. Spectral ratio G_3/G_4 at PAS. (a) Theoretical curve for a 560 km rupture; (b) Theoretical curve for a 270 km rupture; (c) Experimental curve.

Figure 9. Spectral amplitude of observed R_2 trace at PAS. No hole in R_2 is observed at 195 sec., as would be required by the 560 km solution.

Figure 10. Map of the epicentral area of the Gobi-Altai earthquake. The big star shows the epicenter; small dots indicate aftershocks; the rack line represents the isoseismic line of degree 5; the light trace is the 560km rupture fault suggested by BMT62; the heavier trace (displaced South to enhance clarity) is the 270 km fault propsed here.

PRECEDING PAGE BLANK NOT FILMED

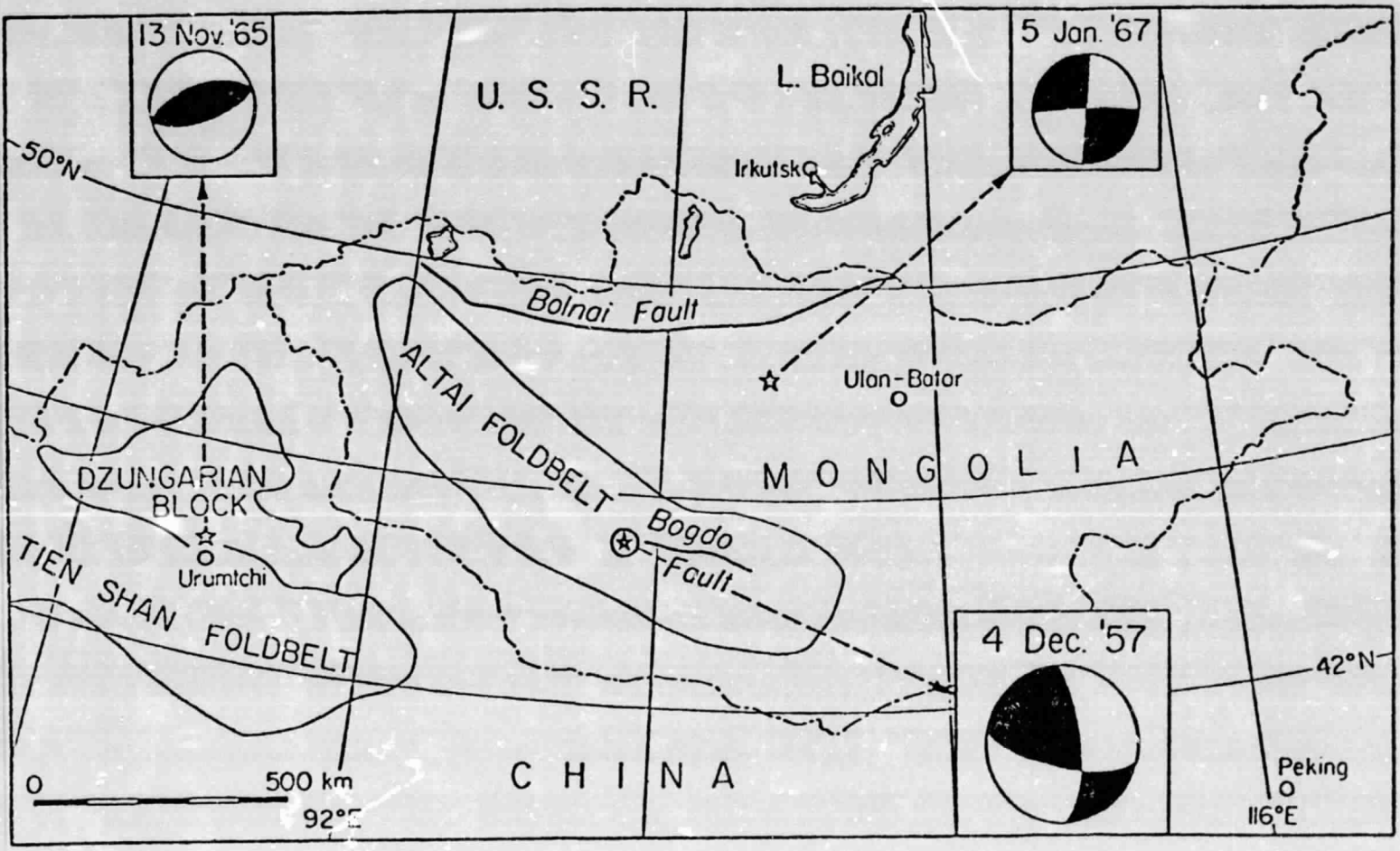

Fig. 1

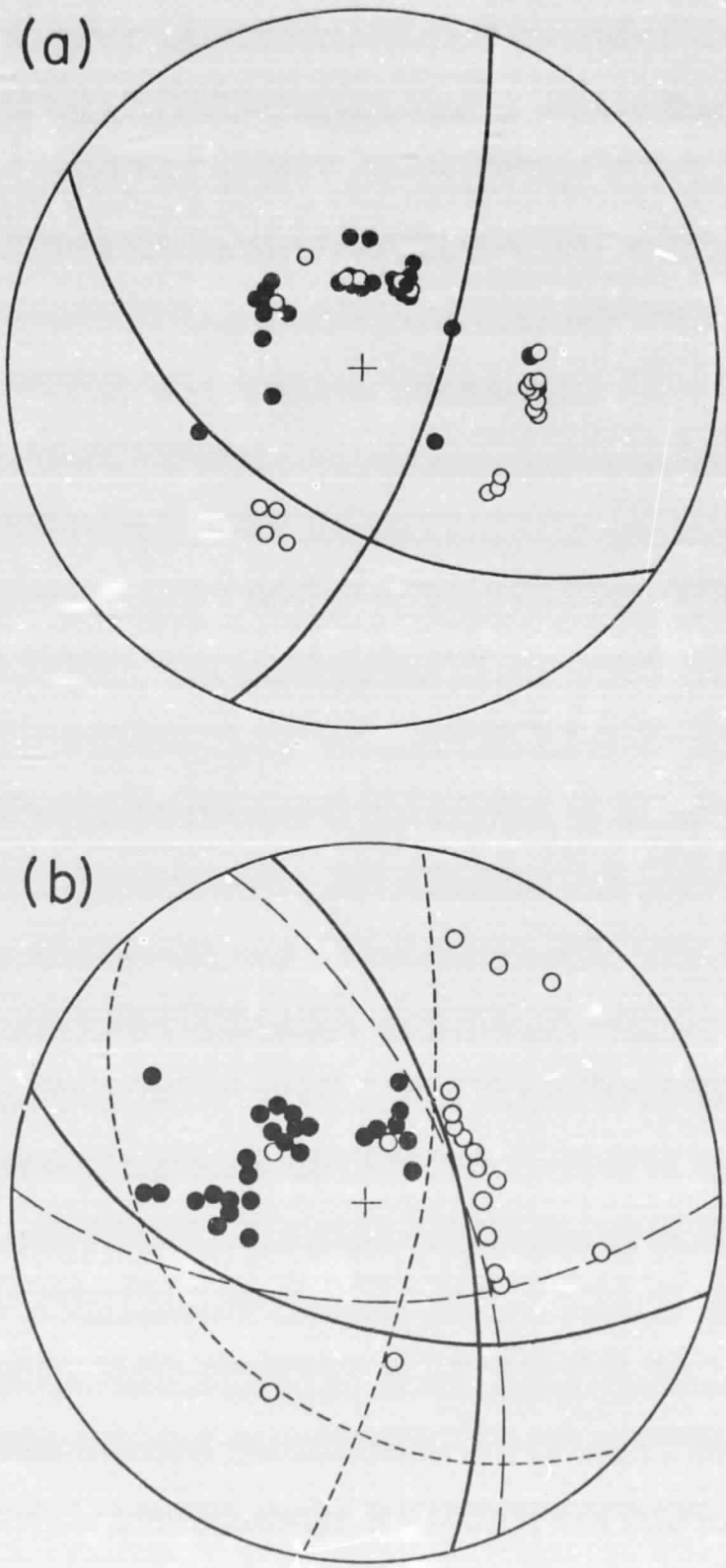

Fig. 2a, b

(c)

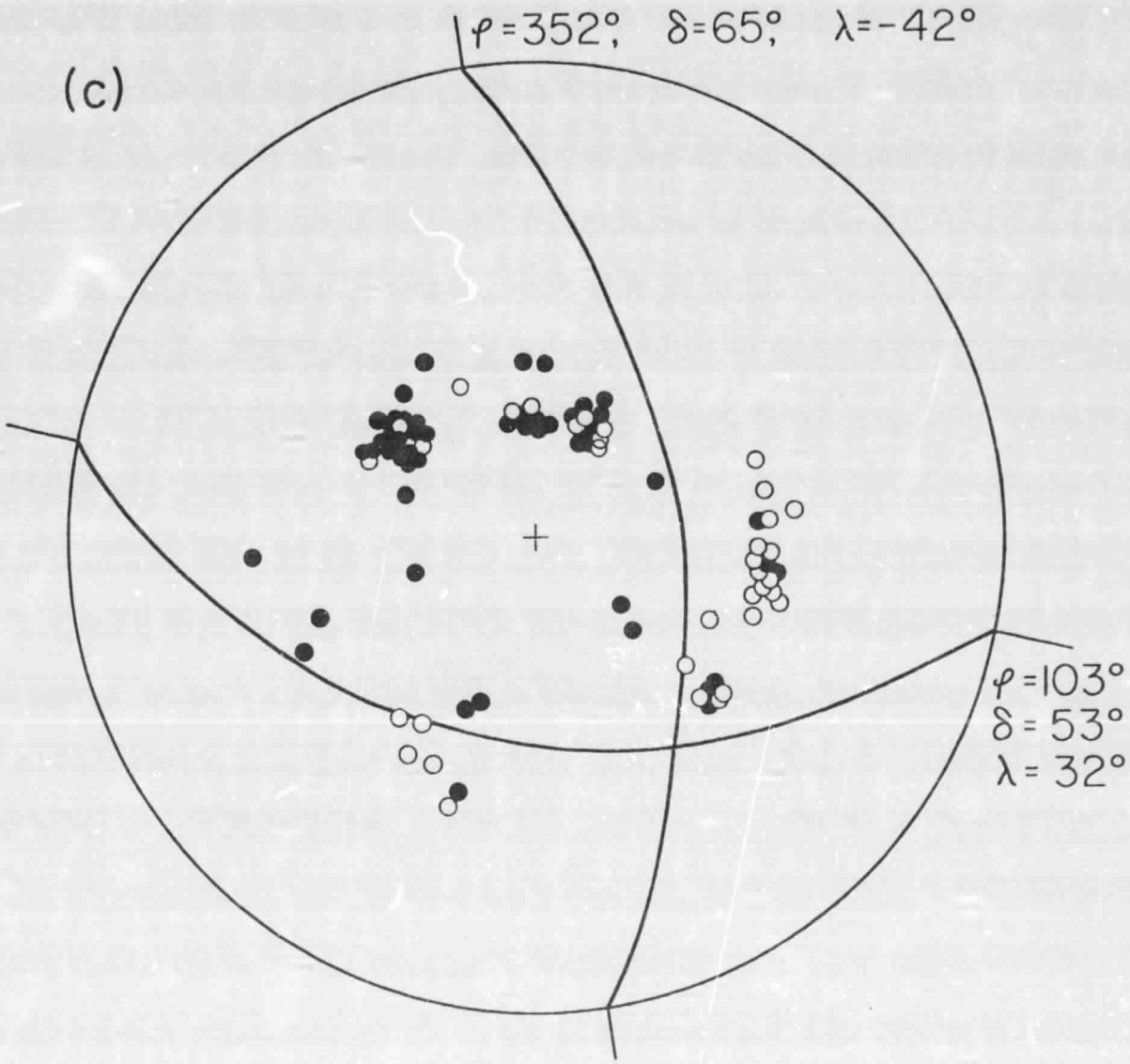

(d)

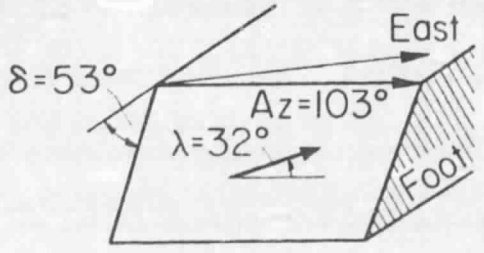

Fig. 2c,d

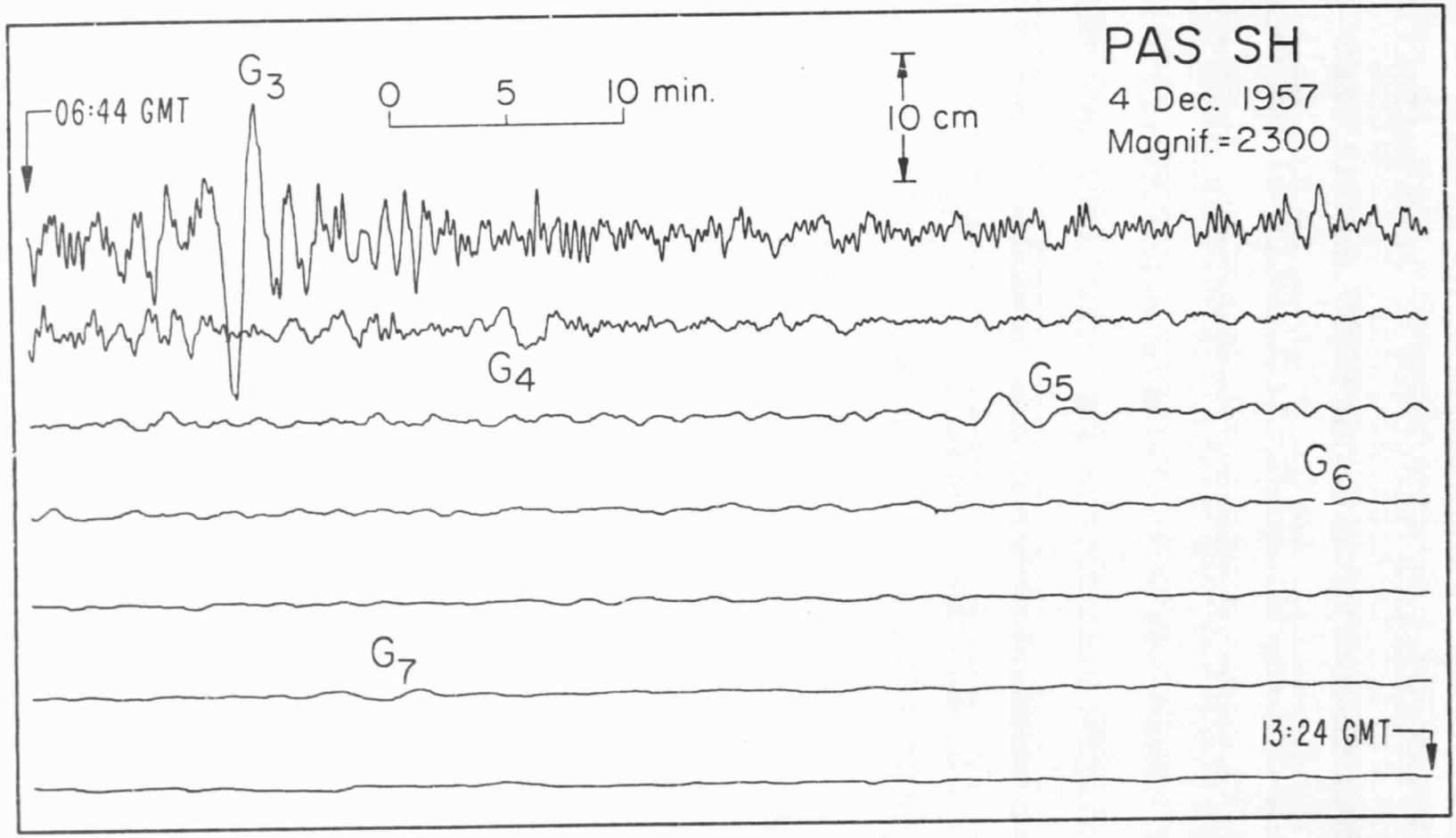
PAS SH
4 Dec. 1957
Magnif.=2300
06:44 GMT
G3
0 5 10 min.
10 cm
G4
G5
G6
G7
13:24 GMT

Fig. 3

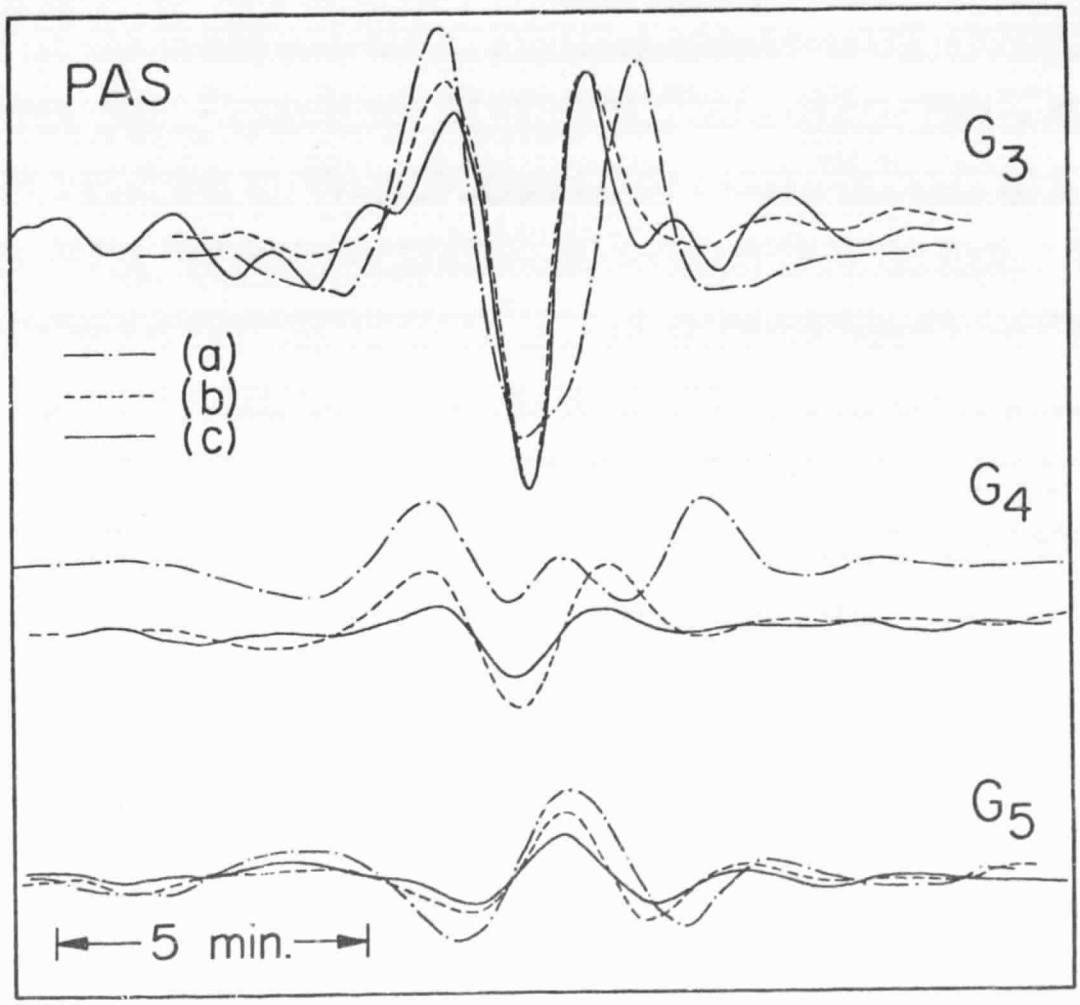

Fig. 4

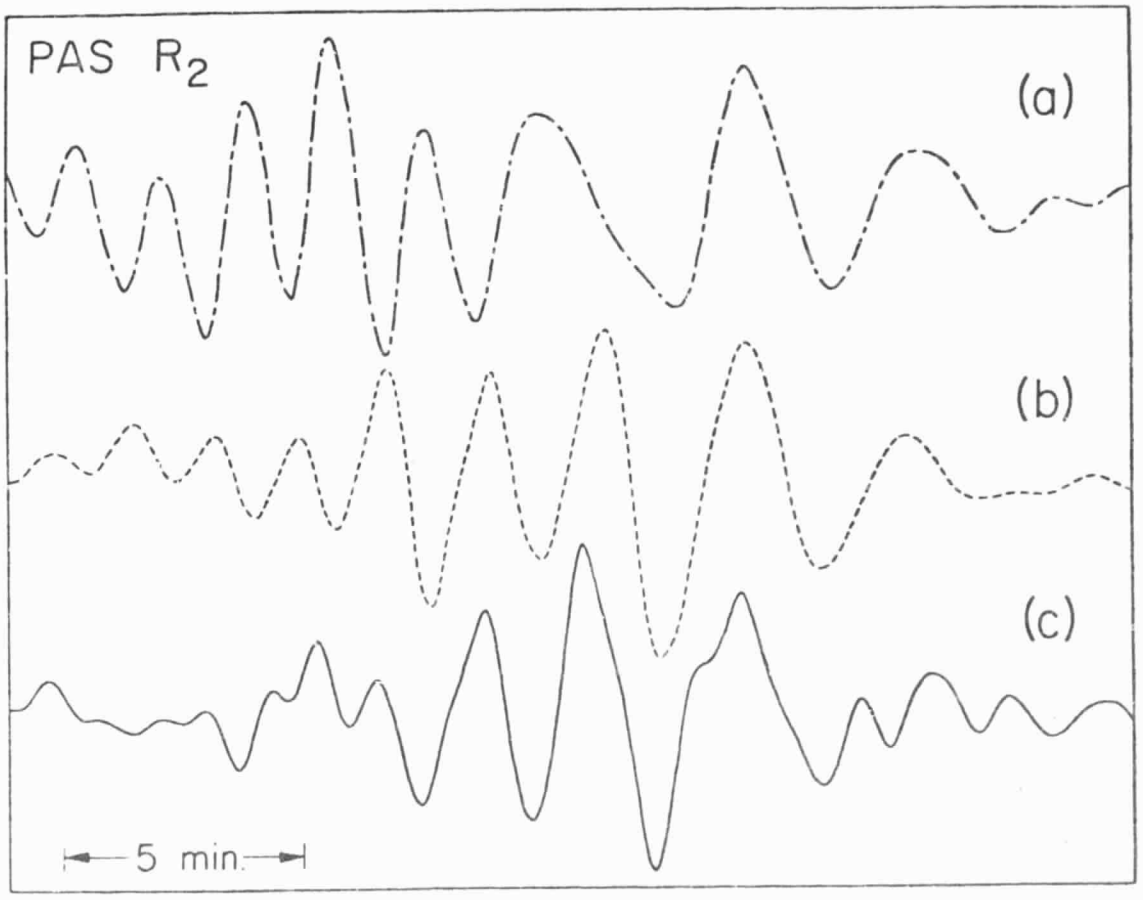

Fig. 5

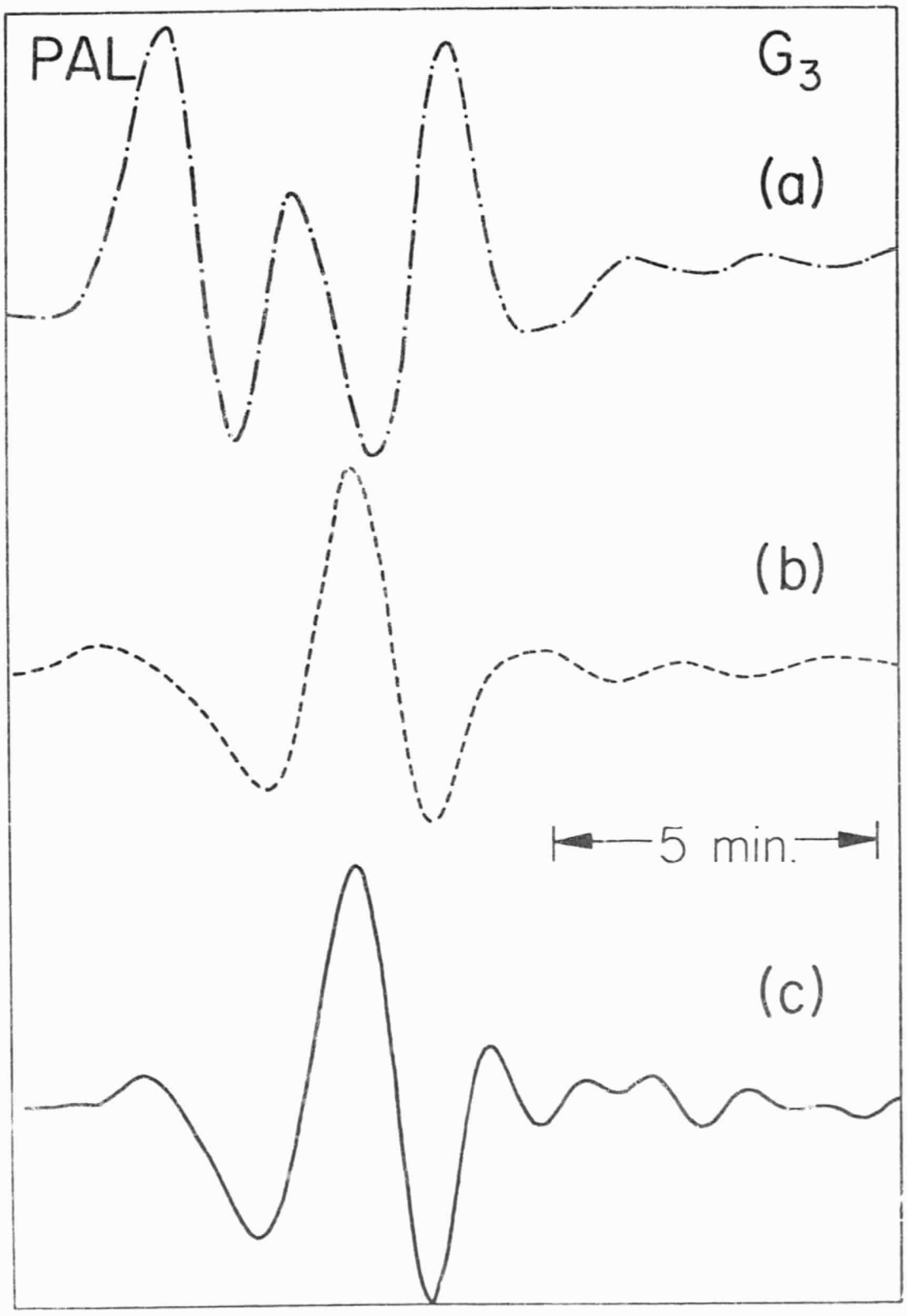

Fig. 6

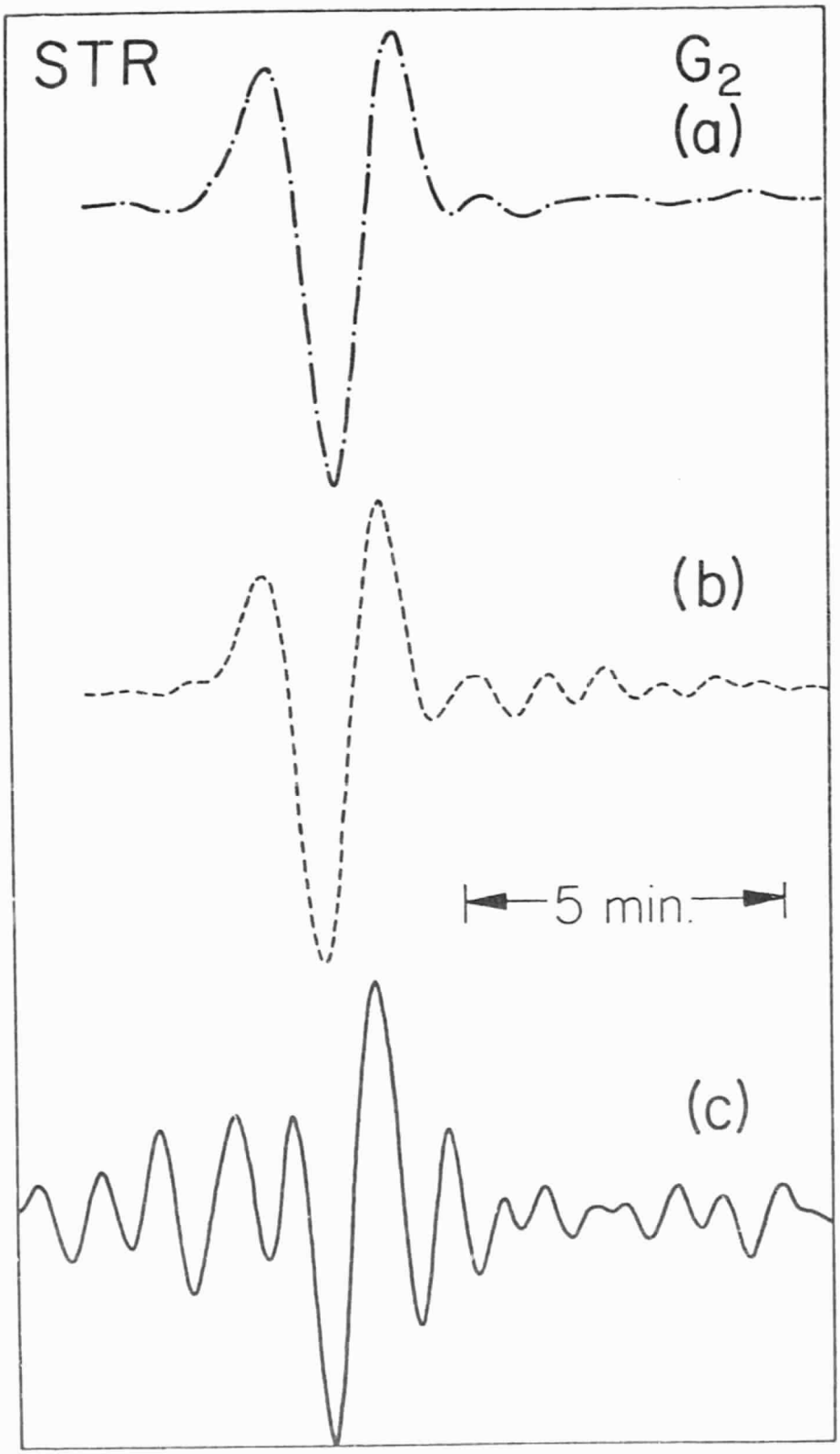

Fig. 7

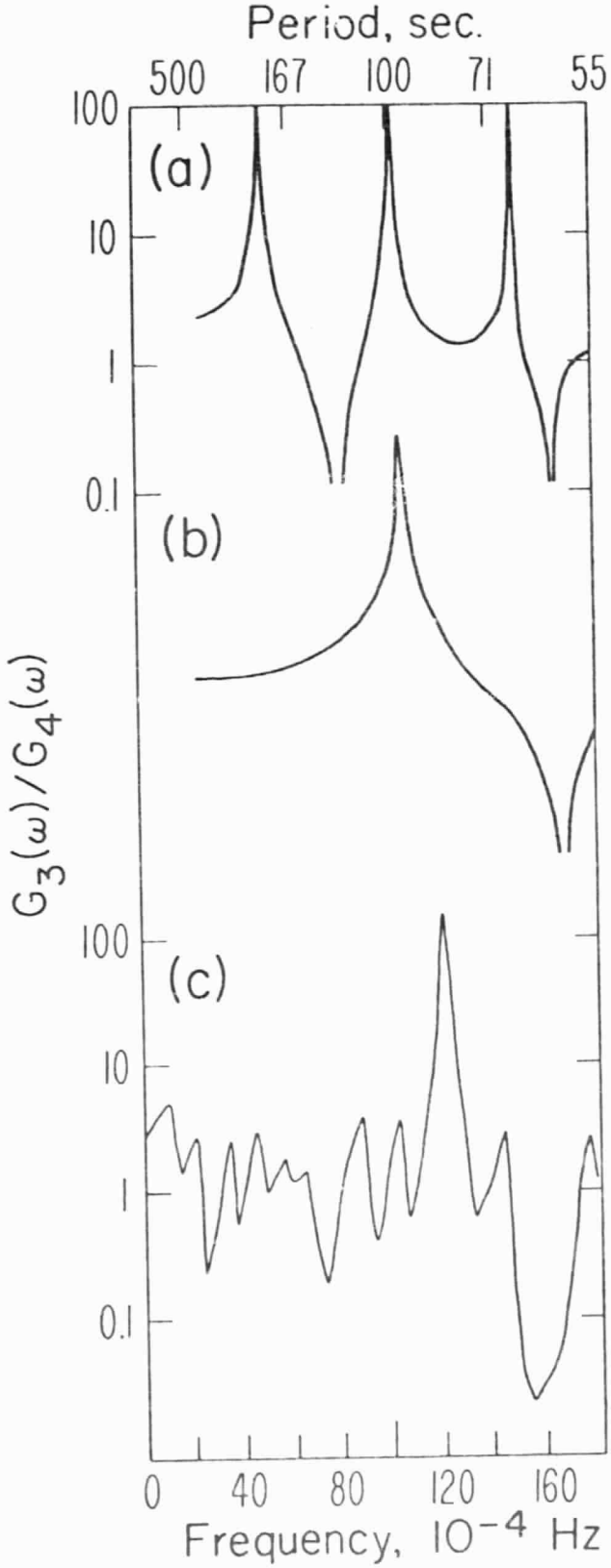
Period, sec.
500
167
100
71
55
100
10
1
0.1
(a)
(b)
(c)
$G_3(\omega)/G_4(\omega)$
100
10
1
0.1
0
40
80
120
160
Frequency, 10^{-4} Hz

Fig. 8

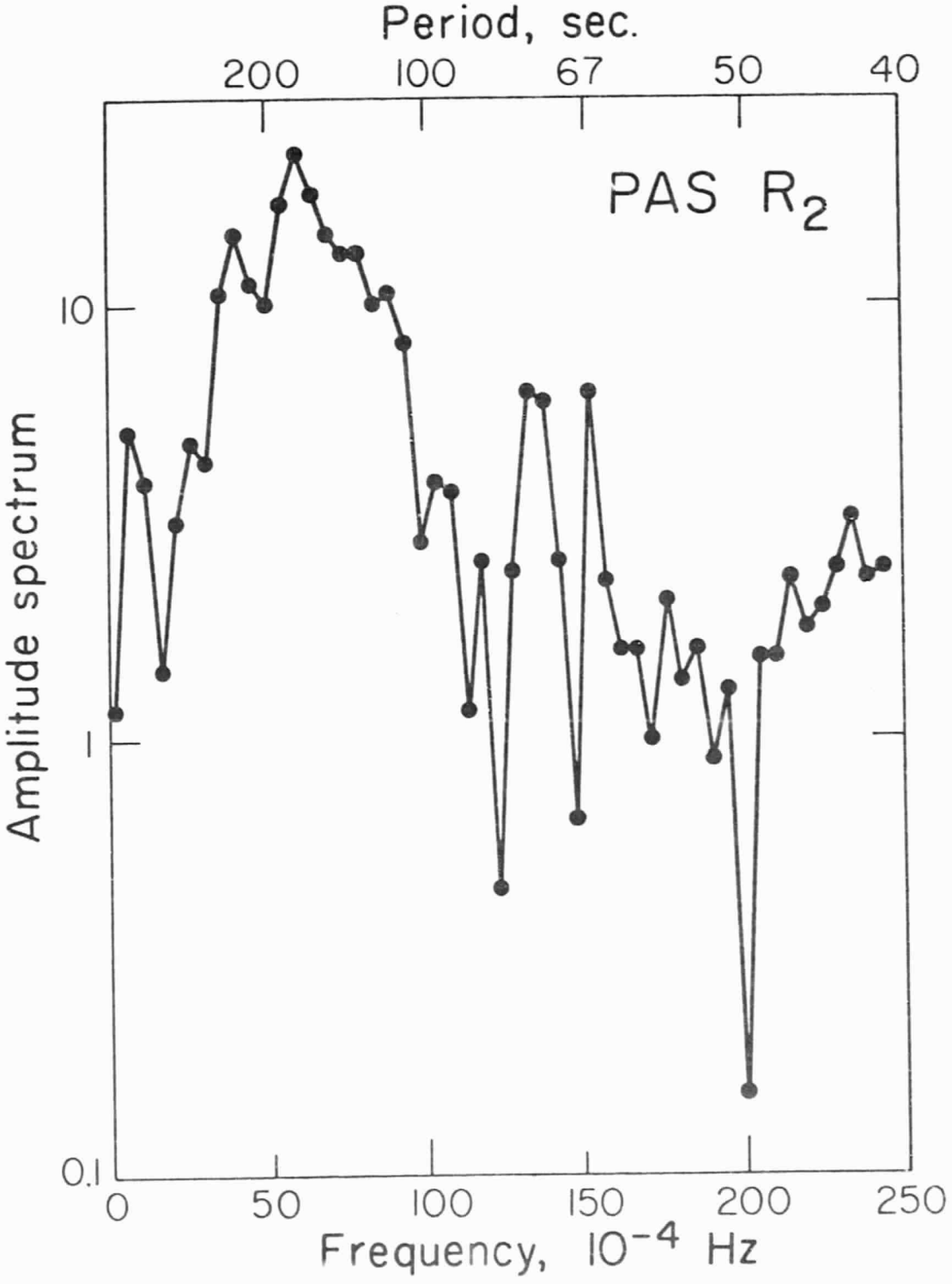
Period, sec.
200
100
67
50
40
PAS R_2
10
1
0.1
Amplitude spectrum
0
50
100
150
200
250
Frequency, 10^{-4} Hz

Fig. 9

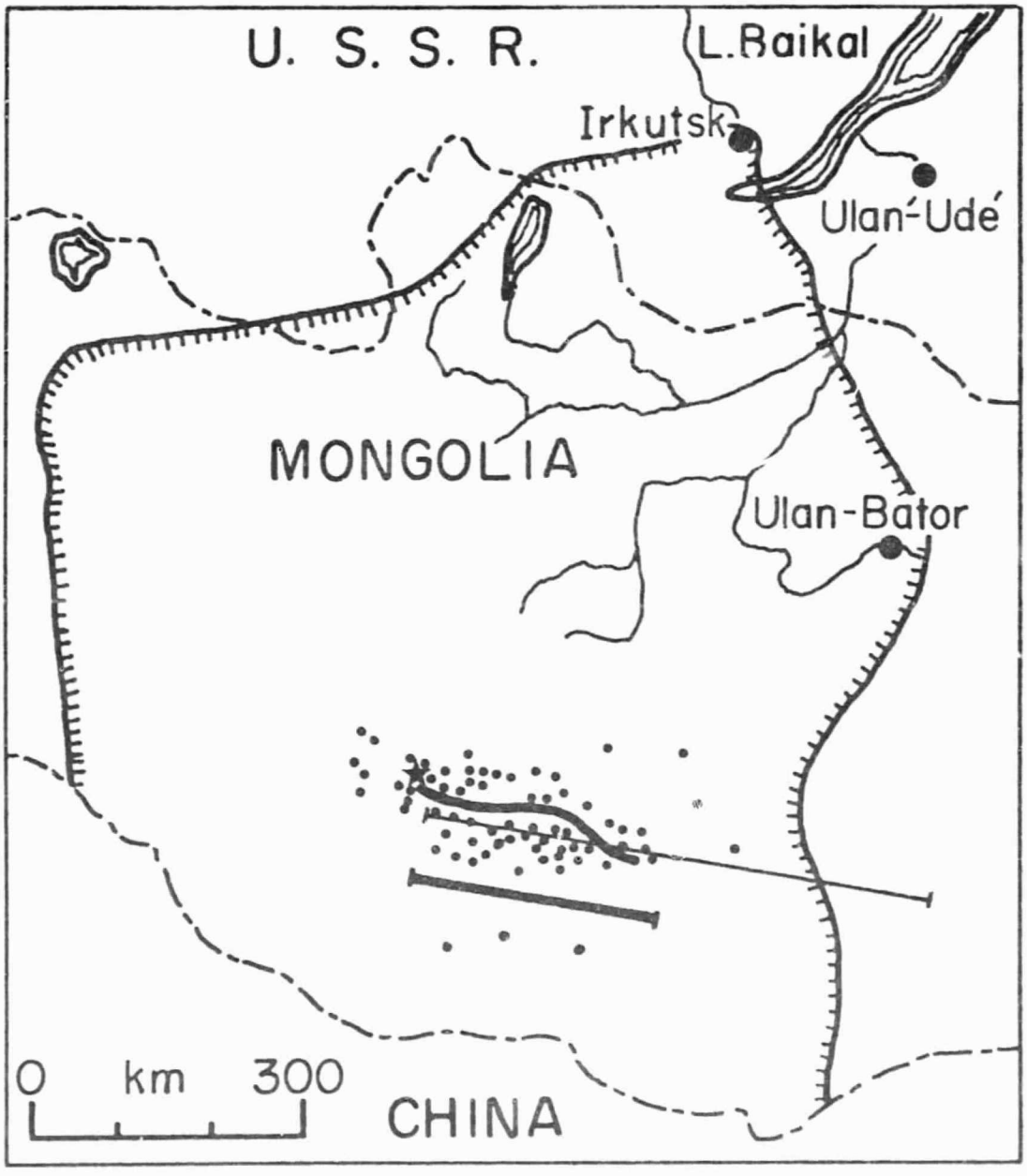
U. S. S. R.
L.Baikal
Irkutsk
Ulan-Udé
MONGOLIA
Ulan-Bator
0 km 300
CHINA

Fig. 10